Frustration-Induced Valence Bond Crystal and Its Melting in Mo_3Sb_7

T. Koyama,[1] H. Yamashita,[1] Y. Takahashi,[1] T. Kohara,[1] I. Watanabe,[2] Y. Tabata,[3] and H. Nakamura[3]

[1]*Graduate School of Material Science, University of Hyogo, Kamigori, Ako-gun, Hyogo 678-1297, Japan*
[2]*Advanced Meson Science Laboratory, RIKEN Nishina Center, Wako 351-0198, Japan*
[3]*Department of Materials Science and Engineering, Kyoto University, Kyoto 606-8501, Japan*

(Received 26 May 2008; published 19 September 2008)

$^{121/123}$Sb nuclear quadrupole resonance and muon spin relaxation experiments of Mo_3Sb_7 revealed symmetry breakdown to a nonmagnetic state below the transition recently found at $T_S \simeq 50$ K. The transition is characterized by a distinct lattice dynamics suggested from narrowing of nuclear fields. We point out that the Mo sublattice is a unique three-dimensional frustrated lattice where nearest-neighbor and next-nearest-neighbor antiferromagnetic interactions compete, and propose that tetragonal distortion to release the frustration stabilizes long-range order of spin-singlet dimers, i.e., valence bond crystal, which is thermally excited to the dynamic state with cubic symmetry.

DOI: 10.1103/PhysRevLett.101.126404 PACS numbers: 71.20.Be, 76.60.−k, 76.75.+i

Exotic phenomena induced by the geometric frustration have attracted great interest, and the attempt to find novel phases has been ongoing [1]. In the case of three-dimensional (3D) pyrochlore lattice, the symmetry breakdown to spin-Peierls-like states or to the valence bond crystal with the quenched spin degrees of freedom [2,3] is one of the options to release the frustration; a typical example is found in the case of $MgTi_2O_4$ [4].

A metallic compound Mo_3Sb_7, with the cubic Ir_3Ge_7 type structure (space group $Im\bar{3}m$), is a superconductor with a critical temperature $T_c \simeq 2.3$ K [5]. The Mo sublattice (12*e*), shown in the inset of Fig. 1(a), is a 3D network of Mo-Mo dumbbells formed by nearest neighbors (NN), while next-nearest-neighbor (NNN) bonds form an octahedral cage at the body-centered position (respective interactions are referred to as J_1 and J_2). The short NN distance (3.0 Å) compared with the NNN distance (4.6 Å) tends to dimerize the NN pairs. On the other hand, in an extreme case with $J_1 = 0$ and $J_2 < 0$, where the negative sign corresponds to antiferromagnetic (AFM) interaction, the typical 3D frustration emerges in the NNN regular octahedron. These facts make us anticipate unusual competition between intradimer and interdimer interactions. Recently, Candolfi *et al.* [6] regarded Mo_3Sb_7 as an itinerant electron system and suggested coexistence of superconductivity and spin fluctuations, which is a rare example in *d* electron metals. A broad maximum in the temperature (T) dependence of the susceptibility (χ), a large electronic specific heat coefficient, a T^2 dependence of low-T electrical resistivity, the Kadowaki-Wood relation between the specific heat and the resistivity, etc., point to the presence of strong electron correlation. Band structure calculations for cubic Mo_3Sb_7 [7,8], showing appreciable contribution of Mo-4*d* orbitals to the density of states near the Fermi level $D(E_F)$, are in agreement with these observations. Although no phase transition other than that at T_c was known in [6], Tran *et al.* [9] reported recently the presence of another phase transition at $T^* \simeq 50$ K (in this Letter, referred to as T_S), and proposed spin gap formation with the magnitude of 120 K associated with Mo-Mo dimerization. In fact at sufficiently high T, χ shows a $S = 1/2$ Curie-Weiss behavior (for Mo^{5+}) with a large negative Weiss temperature, suggesting strong AFM interaction among active Mo spins. Thus the Mo electronic state is of interest as the system with both itinerant and localized characters. Furthermore, Mo_3Sb_7 is now recognized as a new material with another phase transition prior to superconductivity; the pairing mechanism is still controversial [5,8–13].

In this Letter, to study microscopic and dynamic magnetism in Mo_3Sb_7, particularly to identify the phase between T_c and T_S, we present $^{121/123}$Sb nuclear quadrupole resonance (NQR) and muon spin relaxation (μSR) results together with low-T x-ray diffraction (XRD) data. We

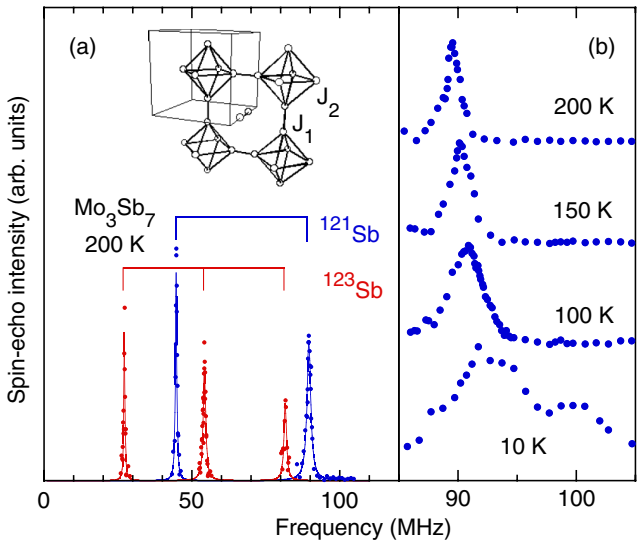

FIG. 1 (color online). (a) $^{121/123}$Sb NQR spectrum of Mo_3Sb_7 at 200 K. Inset shows the Mo sublattice. (b) T variation of ^{121}Sb-$2\nu_Q$ line.

discuss possible frustration in the Mo sublattice by assuming negative J_1 and J_2, and propose new exotic states realized due to competing J_1 and J_2.

Polycrystalline Mo_3Sb_7 specimen were prepared via reaction between liquid Sb and solid Mo. NQR spin-echo measurements were carried out using a conventional phase-coherent-type pulse spectrometer at 1.4–200 K. Zero-field (ZF) μSR measurements were made at the RIKEN-RAL Muon Facility at the Rutherford-Appleton Laboratory using a pulsed positive surface muon beam at 5–250 K. Low-T powder XRD was measured using a conventional diffractometer (MacScience MXP) with Cu $K\alpha$ radiation.

NQR probes both static and dynamic local magnetic field as well as electric field gradient (EFG) at the nuclear site. Figure 1(a) shows the $^{121/123}$Sb NQR spectrum of Mo_3Sb_7 at 200 K. Antimony has two isotopes ^{121}Sb (nuclear spin $I = 5/2$) and ^{123}Sb ($I = 7/2$), which yield two and three quadrupole transition lines, respectively. In cubic Mo_3Sb_7, there are two nonequivalent Sb sites with nonaxial and axial symmetries ($12d$ and $16f$, respectively). We have found only five lines at 200 K corresponding to either site. This is probably because the nuclear spin relaxation rate at the unobserved site is enhanced due to fast fluctuations of active Mo electron spins. The frequency intervals between neighboring lines of $^{121/123}$Sb are approximately equal, indicating nearly axial EFG at the observed site. $^{121/123}$Sb quadrupole frequencies are $^{121/123}\nu_Q \simeq$ 47.7/27.2 MHz at 200 K.

The T dependence of the ^{121}Sb-$2\nu_Q$ line (transitions of $|\pm 3/2\rangle \leftrightarrow |\pm 5/2\rangle$) is shown in Fig. 1(b). The line is shifted to the high frequency side and gradually broadened on cooling towards T_S. At $\sim T_S$, the line loses intensity and disappears due to highly enhanced spin-echo decay rate $1/T_2$ (see the inset of Fig. 2, which will be recalled below). Below 20 K the signal reappears with complicated structures [see the data at 10 K in Fig. 1(b)]. Actually, ZF nuclear resonance signal was continuously observed in almost the whole frequency range below 110 MHz with a number of peaks. This indicates clearly symmetry breakdown below T_S. The origin is either appearance of the internal field (due to magnetic order), separation of crystallographic Sb sites (due to structural deformation), or both. Unfortunately, the spectrum at low T is too complicated and unresolved to conclude this issue because of line split together with broadening, as well as the possible emergence of the signal from another Sb site. An early ^{121}Sb Mössbauer study was not conclusive either [14]. Hence, to determine the magnetic ground state, we employ another microscopic probe, μSR; the result will be presented later.

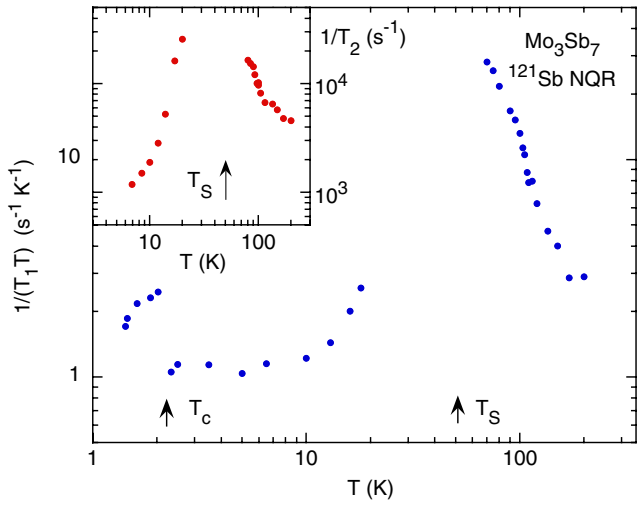

FIG. 2 (color online). T dependence of ^{121}Sb-$1/(T_1T)$ and $1/T_2$ (inset) for Mo_3Sb_7.

The nuclear spin-lattice relaxation rate $1/T_1$, giving information on electron spin fluctuations via hyperfine coupling, was measured for both ^{121}Sb- and ^{123}Sb-$2\nu_Q$ transitions. The ratio of relaxation rates for the different isotopes is $^{123}T_1/^{121}T_1 \simeq 3.5$ at $T > T_S$, being close to the squared gyromagnetic ratios $^{121}\gamma_n^2/^{123}\gamma_n^2 \simeq 3.4$. This confirms that the relaxation process is not by fluctuations of EFG but by those of the internal magnetic field at least above T_S. The T dependence of $1/T_1$ measured for ^{121}Sb is plotted in the form of $1/(T_1T)$ vs T in Fig. 2 [15]. The divergent behavior was observed at $\sim T_S$, although reliable values of $1/T_1$ could not be obtained near T_S due to poor signal-to-noise ratio. In fact, the transition at T_S is characterized by the stronger T dependence of $1/T_2$ (the inset of Fig. 2): $1/T_2 \sim 10$–$10^3(1/T_1)$. This implies the presence of anomaly in the nuclear spin-spin coupling, being rare in the electronic spin transition. Below T_S, $1/(T_1T)$ decreases rapidly with decreasing T, being consistent with the possible existence of spin gap [9], but turns to show a $T_1T =$ const Korringa behavior below $\sim$10 K, indicating the presence of residual $D(E_F)$. $1/T_1$ is enhanced just below T_c, which is known as a coherence peak for the conventional BCS superconductor with an isotropic gap [16].

Now we shift to μSR results. Being different from NQR, μSR probes only the magnetic field, and is very sensitive to the appearance and variation of the internal field. Typical examples of ZF-μSR spectra are shown in the inset of Fig. 3. Even at the lowest T (5 K), no straightforward evidence of magnetic order such as muon spin precession was observed. At all T, the feature of relaxation is essentially the same and shows Gaussian-like depolarization. The commonly used damped Kubo-Toyabe (KT) function $P_\mu(t) = \exp(-\Lambda t)G_z^{\mathrm{KT}}(\Delta, t)$ with $G_z^{\mathrm{KT}}(\Delta, t) = \frac{1}{3} + \frac{2}{3}(1 - \Delta^2t^2)\exp(-\frac{1}{2}\Delta^2t^2)$ was fit to the data, where Δ/γ_μ is the width of the static field distribution (γ_μ the muon gyromagnetic ratio), and Λ is the damping rate associated with an additional relaxation process. As seen below, the KT term is dominated by the nuclear dipolar field H_n and the damping part reflects the Mo electronic system. Figure 3 shows the T dependence of Δ. First, let us see the T-independent part in the intermediate T range of

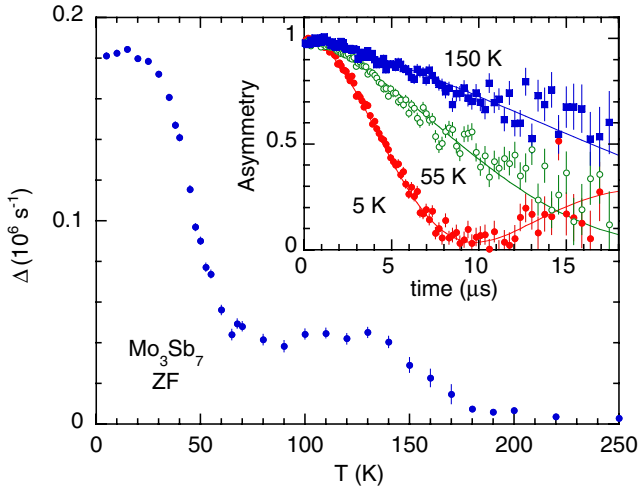

FIG. 3 (color online). T dependence of the ZF Kubo-Toyabe relaxation rate Δ in Mo_3Sb_7. Inset shows typical examples of ZF-μSR spectra (at 5, 55, and 150 K). Solid curves indicate the fit by the damped KT function.

~70–140 K with $\Delta/\gamma_\mu \simeq 0.5$ G. This tiny field is most probably due to dipolar fields coming from randomly oriented nuclear spins. Above ~140 K, Δ is reduced markedly. As shown in Fig. 4, $\ln\Delta$ is in proportion to $1/T$ in the T range, suggesting a motional narrowing process caused by muon hopping among different sites, that is frequently observed at high T. With decreasing T passing through T_S, Δ is enhanced strongly as seen in Fig. 3. The origin of the additional internal field below T_S is the most essential point in this experiment. The Gaussian-type random distribution with small $\Delta/\gamma_\mu \simeq 2.1$ G even at the lowest T is hardly attributed to the electron spin freezing but is reasonably explained as due to the change in H_n associated with the structural deformation mentioned below. The T dependence of Δ at ~T_S is again explained as a thermal excitation process with activation energy of $E_a/k_B \simeq 120$ K. This T variation, without critical divergence, implies that a principal part of field fluctuations is dominated by *dynamic* process of nuclear spins, i.e., of lattice. In other words, electron spin fluctuations, which should show a critical behavior at T_S, is relatively less enhanced at the muon site. This result gives very fruitful information on the nature of the transition at T_S, as discussed below.

The T dependence of Λ, which also gives information on the Mo electronic spin fluctuations as NQR-$1/T_1$, is shown in the inset of Fig. 4. The decrease above ~150 K would be an analytical artifact due to the evolution of the relaxation process associated with the dynamic muon hopping. Λ has a sharp peak at T_S and decreases rapidly below T_S. This behavior is qualitatively the same as that of NQR-$1/T_1$. The quantitative difference in NQR-$1/T_1$ and μSR-Λ is most probably due to the difference in the coupling mechanism; the interaction between Sb nuclei and Mo electrons is probably dominated by the direct hyperfine coupling, while fields from Mo electrons to the muon site are by the dipolar mechanism. Different time windows of the measurements would also be appreciable. Furthermore, the muon stopping site may be a high symmetric position, say the center of the Mo cage, where the fields from Mo electron spins would mostly be canceled.

To get information on the lattice symmetry below T_S, we made conventional XRD analyses at low T and found appreciable difference in the patterns below and above T_S. To see the change efficiently, we particularly show (600) diffraction peaks at 70 and 15 K in Fig. 5(a) [17]. A high-T singlet splits into double peaks with the intensity ratio of ~2:1 by crossing T_S, suggesting structural deformation from cubic to tetragonal (space group $I4/mmm$) as

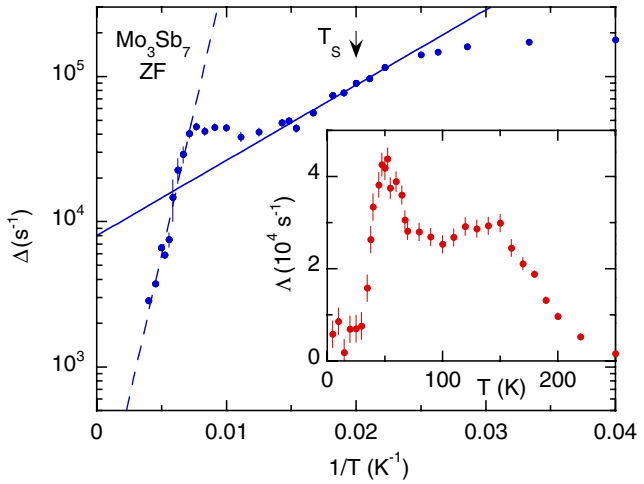

FIG. 4 (color online). ZF Kubo-Toyabe relaxation rate Δ in Mo_3Sb_7 plotted against $1/T$. Activation energies for two different thermal excitation processes are estimated to be 120 and 910 K from the solid line and broken line, respectively. Inset shows T dependence of the relaxation rate Λ.

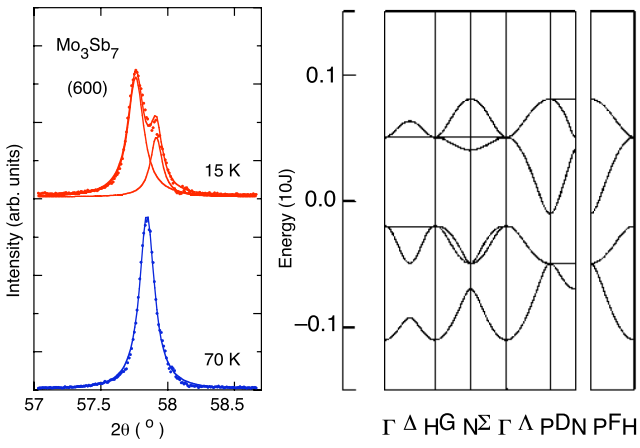

FIG. 5 (color online). (a) X-ray (600) peak of Mo_3Sb_7 at 70 K and its split pattern at 15 K [17]. The $K\alpha_2$ contribution is subtracted by profile fitting. (b) Dispersion curves of the exchange integral $J(q)$ of the Mo sublattice assuming negative J_1 and J_2. $J_1 = -0.05$ and $J_2 = 0.3J_1$ were used arbitrarily.

the simplest possibility; the lattice parameter a is larger than c by $\sim 0.2\%$ at 15 K.

Although Mo_3Sb_7 is a metallic magnet, here we focus on the local nature of the Mo electron. Taking a look at the Mo sublattice, if J_1 is dominant, no substantial symmetry breakdown is necessary to form dimers since Mo-Mo dumbbells run along [100], [010], and [001] equally. Therefore in discussing the mechanism of the transition, the low-T lattice symmetry is essential and J_2 should be taken into account. Note that positive J_2 as suggested in [9] does not destabilize the cubic state. Here assuming negative J_1 and J_2, we calculated eigenvalues of their Fourier transform $J(q)$ for the cubic state in the scheme of the linear combination of atomic orbitals approximation; see Fig. 5(b). A flat dispersion of $J(q)$ found along the highest P-(D)-N branch indicates macroscopic degeneracies of AFM ground states [18]; the Mo sublattice is not fully frustrated like pyrochlore but is frustrated for all AFM states with $\mathbf{q} = (\frac{1}{2}\ \frac{1}{2}\ \xi)$ with arbitrary ξ. We also confirmed that the suggested tetragonal deformation lifts the degeneracies. Thus we conclude that the cubic structure is unstable for negative J_2. The lattice deformation may be spin-frustration-driven symmetry breakdown like the spin Jahn-Teller (JT) effect [2]. The strong T dependence of $1/T_1$ at $\sim T_S$, being unlikely for a classical JT transition, suggests enhanced spin fluctuations and the spin-driven mechanism. In Mo_3Sb_7, the spin frustration triggers the tetragonal deformation to decouple the 3D isotropic AFM interaction, and stabilizes spatial long-range order of spin-singlet dimers, i.e., the valence bond crystal. As the reduced χ from higher T ($\gg T_S$) and the considerably broadened specific heat (C) anomaly were reported [9], this state is realized instead of long-range AFM order due to strong intradimer coupling already developed from sufficiently high T.

Taking account of the motional narrowing of H_n observed by μSR at $\sim T_S$, and structural characteristics of the low-T phase, we propose a scenario for the transition. First, note that the deformed states along the [100], [010], and [001] directions are degenerate; we refer to the corresponding Mo electronic states as ψ_x, ψ_y, and ψ_z. We expect that the high-T cubic state is the dynamic mixing of the three states, i.e., $(\psi_x + \psi_y + \psi_z)/\sqrt{3}$, just like the vibronic dynamic JT state. In other words, harmonic oscillations of the valence bonds keeping strong intradimer interaction are thermally induced. The narrowing of μSR-Δ, which reflects a relatively high-energy part of the dynamics, is explained naturally; at sufficiently low T, muons sense well-defined H_n from the deformed Mo sublattice, which are averaged by the dynamic atomic motion with increasing T. NQR-$1/T_2$ above T_S, which nearly follows μSR-Δ, is explained by the same mechanism, while the damping below T_S is ascribed to the decoupling of the nuclear spin-spin interaction, i.e., the reduction of Sb-like nuclei due to the separation of the Sb sites in the distorted state.

In conclusion, NQR and μSR experiments revealed symmetry breakdown to a nonmagnetic state below $T_S \simeq 50$ K, with most probably tetragonal lattice distortion. Assuming negative J_1 and J_2 in the Mo sublattice, we pointed out possible frustration and proposed long-range order of spin-singlet dimers to the valence bond crystal, which transfers to the characteristic dynamic state with the cubic symmetry above T_S. The electron itinerancy and the present description focusing on the local nature should be reconciled in further studies, similarly to in other geometrically frustrated metals [19].

We acknowledge T. Mito and K. Ueda for helpful discussions, Y. Narumi and K. Kindo at ISSP, the University of Tokyo, and Y. Tanaka at RIKEN, SPring-8 for collaboration. This work was supported by a grant from the University of Hyogo, and by Grant-in-Aid for Scientific Research on Priority Areas "Novel States of Matter Induced by Frustration" (19052003) from MEXT, Japan.

[1] A. P. Ramirez, in *Handbook of Magnetic Materials*, edited by K. H. J. Buschow (North-Holland, Amsterdam, 2001).
[2] Y. Yamashita and K. Ueda, Phys. Rev. Lett. **85**, 4960 (2000).
[3] O. Tchernyshyov *et al.*, Phys. Rev. B **66**, 064403 (2002).
[4] M. Isobe and Y. Ueda, J. Phys. Soc. Jpn. **71**, 1848 (2002); M. Schmidt *et al.*, Phys. Rev. Lett. **92**, 056402 (2004); S. Di Matteo *et al.*, Phys. Rev. Lett. **93**, 077208 (2004).
[5] Z. Bukowski *et al.*, Solid State Commun. **123**, 283 (2002).
[6] C. Candolfi *et al.*, Phys. Rev. Lett. **99**, 037006 (2007).
[7] U. Häussermann *et al.*, Chem. Eur. J. **4**, 1007 (1998); E. Dashjav *et al.*, J. Mater. Chem. **12**, 345 (2002).
[8] V. H. Tran *et al.*, arXiv:0803.2948v1.
[9] V. H. Tran *et al.*, Phys. Rev. Lett. **100**, 137004 (2008).
[10] V. M. Dmitriev *et al.*, Supercond. Sci. Technol. **19**, 573 (2006).
[11] C. Candolfi *et al.*, Phys. Rev. B **77**, 092509 (2008).
[12] R. Khasanov *et al.*, Phys. Rev. B **78**, 014502 (2008).
[13] V. M. Dmitriev *et al.*, Low Temp. Phys. **33**, 295 (2007).
[14] J. D. Donaldson *et al.*, Acta Chem. Scand. A **28**, 866 (1974).
[15] Nuclear magnetization recovery was fitted well using the multiexponential function with a single parameter expected for the case of axial EFG [D. E. MacLaughlin and J. D. Williamson, Phys. Rev. B **4**, 60 (1971)]. Below T_S, $1/T_1$ was measured at the peak position near 90 MHz. The same recovery function for axial EFG was used only for simplicity.
[16] L. C. Hebel and C. P. Slichter, Phys. Rev. **113**, 1504 (1959).
[17] In fact, the (600) reflection is superimposed with (442), of which intensity is smaller by one order.
[18] A. B. Harris *et al.*, Phys. Rev. B **45**, 2899 (1992); J. N. Reimers *et al.*, Phys. Rev. B **43**, 865 (1991).
[19] R. Ballou *et al.*, Phys. Rev. Lett. **76**, 2125 (1996); H. Nakamura *et al.*, J. Phys. Condens. Matter **9**, 4701 (1997); S. Kondo *et al.*, Phys. Rev. Lett. **78**, 3729 (1997).